PNAS RESEARCH ARTICLE | CELL BIOLOGY

Chromatin regulates alternative polyadenylation via the RNA polymerase II elongation rate

Joseph V. Geisberg[a,1], Zarmik Moqtaderi[a,1], and Kevin Struhl[a,2]

Contributed by Kevin Struhl; received March 22, 2024; accepted April 15, 2024; reviewed by John T. Lis and Ali Shilatifard

The RNA polymerase II (Pol II) elongation rate influences poly(A) site selection, with slow and fast Pol II derivatives causing upstream and downstream shifts, respectively, in poly(A) site utilization. In yeast, depletion of either of the histone chaperones FACT or Spt6 causes an upstream shift of poly(A) site use that strongly resembles the poly(A) profiles of slow Pol II mutant strains. Like slow Pol II mutant strains, FACT- and Spt6-depleted cells exhibit Pol II processivity defects, indicating that both Spt6 and FACT stimulate the Pol II elongation rate. Poly(A) profiles of some genes show atypical downstream shifts; this subset of genes overlaps well for FACT- or Spt6-depleted strains but is different from the atypical genes in Pol II speed mutant strains. In contrast, depletion of histone H3 or H4 causes a downstream shift of poly(A) sites for most genes, indicating that nucleosomes inhibit the Pol II elongation rate in vivo. Thus, chromatin-based control of the Pol II elongation rate is a potential mechanism, distinct from direct effects on the cleavage/polyadenylation machinery, to regulate alternative polyadenylation in response to genetic or environmental changes.

alternative polyadenylation | chromatin | RNA polymerase II | transcription elongation | histone chaperones

Significance

Alternative polyadenylation generates numerous 3′ mRNA isoforms, and it can be regulated on a transcriptome scale by environmental or developmental conditions. The Pol II (polymerase II) elongation rate influences poly(A) site selection, with slow and fast Pol II derivatives causing upstream and downstream shifts, respectively, in poly(A) site utilization. Independent depletion of the histone chaperones FACT or Spt6 in yeast cells causes an overall upstream shift, indicating that Spt6 and FACT stimulate the Pol II elongation rate. Conversely, depletion of histone H3 or H4 causes an overall downstream shift, indicating that nucleosomes inhibit the Pol II elongation rate. Thus, chromatin-based control of the Pol II elongation rate is a potential mechanism to regulate alternative polyadenylation in response to genetic or environmental changes.

Unlike prokaryotic RNA polymerases that transcribe simple DNA templates, eukaryotic RNA polymerases transcribe DNA wrapped with nucleosomes. In yeast cells, the RNA polymerase II (Pol II) elongation rate is ~1.5 kb/min, as measured by blocking transcriptional initiation of a Gal4-dependent promoter by glucose repression and following Pol II occupancy across a long gene as a function of time (1). The elongation rate is related to, but distinct from, Pol II processivity, the ability of Pol II to transcribe the entire length of the gene (1). Pol II mutants with reduced elongation rate also have reduced processivity, but mutations in Spt4 or THO complex components reduce processivity without affecting elongation rate (1).

In mammalian cells, transcriptional elongation control plays an important role in developmental gene expression, aging, and disease (2). Pol II elongation rates have been measured on a genomic scale by blocking Pol II pause release with DRB and following Pol II occupancy across all genes as a function of time (3). The median Pol II elongation rate is roughly comparable to that in yeast cells, but it is regulated within genes, across different genes, and in response to environmental stimuli (4–6). Pol II speed affects the dwell time at individual nucleotides throughout the gene and hence cotranscriptional processes such as splicing or polyadenylation (7, 8).

During transcriptional elongation, nucleosomes are in a highly dynamic equilibrium with all four histones being evicted and deposited upon passage of Pol II (9–11). FACT and Spt6 are histone chaperones that travel with elongating Pol II and are important for the rapid eviction and deposition of histones upon transcriptional elongation (12–14). FACT or Spt6 mutations can cause internal initiation within coding regions (15, 16) and mislocalized histone modifications (17). Spt6, along with Spt4/5 (also known as DSIF) and the Paf complex, is a component of the Pol II elongation complex that forms a "cradle" at the DNA exit site (18). FACT recognizes subnucleosome intermediates during transcription and forms an interface with the elongation complex (18). In vivo, Spt6 stimulates the Pol II elongation rate (19), but it is unclear whether this is also true for FACT (14).

The rate of Pol II elongation regulates the profiles of poly(A) sites in yeast (20–22) and human (22–25) cells. Pol II derivatives with slow elongation rates confer upstream-shifted poly(A) profiles, whereas fast Pol II strains confer downstream-shifted poly(A) profiles. These Pol II speed mutants do not generate new poly(A) sites but rather alter their relative utilization. The shifts in poly(A) profiles are due to Pol II speed and not Pol II processivity because cells lacking Spt4 or THO complex components have normal poly(A) profiles, even though they have reduced Pol II processivity (20). The upstream and downstream shifts in poly(A) profiles occur continuously from one isoform to the next, even when isoforms are separated by a single nucleotide (22). This indicates that the cleavage/

Author affiliations: [a]Department of Biological Chemistry and Molecular Pharmacology, Harvard Medical School, Boston, MA 02115

Author contributions: J.V.G., Z.M., and K.S. designed research; J.V.G. and Z.M. performed research; J.V.G., Z.M., and K.S. analyzed data; and J.V.G., Z.M., and K.S. wrote the paper.

Reviewers: J.T.L., Cornell University; and A.S., Northwestern University.

The authors declare no competing interest.

[1]J.V.G. and Z.M. contributed equally to this work.

[2]To whom correspondence may be addressed. Email: kevin@hms.harvard.edu.

This article contains supporting information online at https://www.pnas.org/lookup/suppl/doi:10.1073/pnas.2405827121/-/DCSupplemental.

Published May 15, 2024.

polyadenylation and Pol II elongation complexes are spatially, and perhaps physically, coupled in vivo, strongly suggesting that polyadenylation occurs rapidly upon emergence of the nascent RNA from the Pol II elongation complex (22).

The observations above indicate that poly(A) profiles provide a useful, though indirect, approach to analyze the Pol II elongation rate. Detailed poly(A) profiles involving numerous 3′ mRNA isoforms are easily analyzed on a transcriptome scale. This approach is particularly useful for studying the Pol II elongation rate in yeast cells, which has never been done at the transcriptome scale. Such analysis has been difficult in yeast due to the lack of drugs that specifically inhibit Pol II initiation and because depletion of essential Pol II initiation factors (e.g., TFIIB) takes too long to permit kinetic analysis of Pol II elongation.

Poly(A) site utilization can be regulated on a transcriptome scale by environmental or developmental conditions (26). For example, cancer cells and pluripotent stem cells preferentially express shorter 3′ mRNA isoforms, whereas differentiated cells preferentially express longer 3′ mRNA isoforms (27–32). Such regulation of alternative polyadenylation can have profound phenotypic effects because different 3′ isoforms often have different functional properties. For example, shorter 3′ mRNA isoforms often lack microRNA binding sites that are present in longer isoforms of the same gene and that can repress expression of that gene. Mechanistically, transcriptome-scale regulation of poly(A) profiles can be due to regulated expression or activity of components of the cleavage/polyadenylation machinery (26, 33, 34). In yeast, shorter isoforms are favored under diauxic conditions, likely due to a reduction in the Pol II elongation rate when nucleotide precursors are limiting (20).

Here, we show that depletion of FACT or Spt6 causes upstream-shifted poly(A) profiles of most genes, indicating that these histone chaperones are important to achieve the physiological Pol II elongation rate. Conversely, depletion of histones causes downstream-shifted profiles, indicating that nucleosomes inhibit the Pol II elongation rate. We suggest that chromatin-based control of the Pol II elongation rate is a potential mechanism, distinct from direct effects on the cleavage/polyadenylation machinery, to regulate alternative polyadenylation in response to genetic or environmental changes.

Results

Depletion of FACT or Spt6 Causes an Upstream-Shifted Poly(A) Profile. FACT is a heterodimer of Spt16 and Pob3 (35, 36), and Spt6 interacts strongly with Spn1, another histone chaperone (37, 38). As Spt16 and Spt6 are essential for yeast cell growth, we examined poly(A) profiles in cells individually depleted for these proteins by the anchor-away technique (39). Poly(A) profiles were generated by the 3′ READS technique (40) and analyzed as described previously (20, 22). Biological replicates are highly reproducible (*SI Appendix*, Fig. S1).

On an overall basis, cells depleted of Spt16 (subsequently referred to as FACT) or Spt6 show an upstream-shifted poly(A) profile resembling those observed in two slow Pol II mutants and in wild-type cells grown in diauxic conditions. Fig. 1*A* shows poly(A) profiles of two example genes, and Fig. 1*B* shows a transcriptome-level plot in which boxes demarcate the genome-wide median poly(A) site positions (10th to 90th percentile) relative to the stop codon and vertical bars indicate the median weighted average poly(A) site. In contrast, median poly(A) profiles are not upshifted in cells lacking other proteins involved in Pol II elongation: TFIIS, an elongation factor that stimulates Pol II to cleave RNA to help arrested elongation complexes to resume transcription (41–43); Hpr1, a component of the THO complex that links Pol II elongation to mRNA export (44); Spt4, a component of DSIF (18). Cells lacking Paf1, a subunit of the Paf1 complex that is part of the Pol II elongation complex (18, 45) and is required for methylation of histone H3 at lysines 4 and 79 and ubiquitination of histone H2B at lysine 123 (46, 47), show a very slight upstream shift. Simultaneous depletion of both Spt6 and FACT causes an upstream-shifted poly(A) profile similar in magnitude to that of the individual depletions (Fig. 1*B*).

Spt4 and the THO complex are important for Pol II processivity but not elongation rate (1, 20), and the corresponding mutants do not affect the poly(A) profile (1). Therefore, the upstream-shifted poly(A) profiles in FACT- and Spt6-depleted cells indicate a reduced Pol II elongation rate rather than simply a processivity defect per se. Consistent with a reduced elongation rate, Spt6- and FACT-depleted cells also show reduced Pol II processivity (see later).

Depletion of FACT or Spt6 Causes Increased Polyadenylation in Protein-Coding Regions. Polyadenylation in yeast coding regions occurs at a frequency of ~1% of that occurring in 3′ untranslated regions (3′ UTRs), even though coding regions are several times larger (48–50). In principle, this observation could reflect infrequent polyadenylation in coding regions and/or low stability of the corresponding 3′ isoforms. Although low steady-state expression levels of individual 3′ isoforms terminating in the coding region preclude analysis of their half-lives, decay rates of 3′ isoforms with poly(A) sites in the coding region vs. the 3′ UTR can be compared on an overall basis.

Analysis of published mRNA stability data (51) reveals that the ratio of 3′ isoforms with poly(A) sites in coding regions vs. 3′ UTRs is relatively uniform across a 2 h time course after Pol II depletion (Fig. 2*A*). During this timeframe, most 3′ UTR-terminating isoforms exhibit a >10-fold drop in mRNA levels (51). This observation suggests that 3′ isoforms that are polyadenylated in coding regions have half-lives roughly comparable to those of isoforms with poly(A) sites in 3′ UTRs. Thus, on an overall basis, the low level of poly(A) sites within coding regions reflects a low level of polyadenylation, not decreased stability of these isoforms.

Depletion of FACT or Spt6 results in increased polyadenylation in coding regions (Fig. 2*B*). Similar results are observed in slow Pol II mutant strains as well as the wild-type strain grown in diauxic conditions, but not in strains deleted for Paf1, TFIIS, Hpr1, and Spt4. The relationship between increased polyadenylation in coding regions and upstream shifts in the 3′ UTR (Fig. 2*B*) suggests that these two phenotypes have the same underlying cause. As Pol II traverses the coding region and 3′ UTR, we suggest that increased Pol II dwell time results in increased polyadenylation at more upstream positions. As the cleavage step required for polyadenylation also initiates transcriptional termination (52–55), it occurs only once per newly synthesized RNA molecule, thereby reducing polyadenylation at more downstream positions.

Most Genes Have Upstream-Shifted Poly(A) Profiles in Each of the Three Conditions of Slow Pol II Elongation. We compared the poly(A) profiles of individual genes in FACT-depleted, Spt6-depleted, and slow Pol II (Rpb1-H1085Q) cells by calculating the shift (either upstream or downstream) from the wild-type condition (20). For each of the three genetic conditions, most genes (64 to 84%) show an upstream shift (Fig. 3*A*). Furthermore, in all pairwise comparisons, there is a very strong overlap of genes with upstream-shifted poly(A) profiles (Fig. 3*B*), indicating that these genes are generally sensitive to the Pol II elongation rate. The overlaps between upstream-shifted genes are significantly greater than expected by chance and are particularly strong for FACT-depleted vs. Spt6-depleted cells.

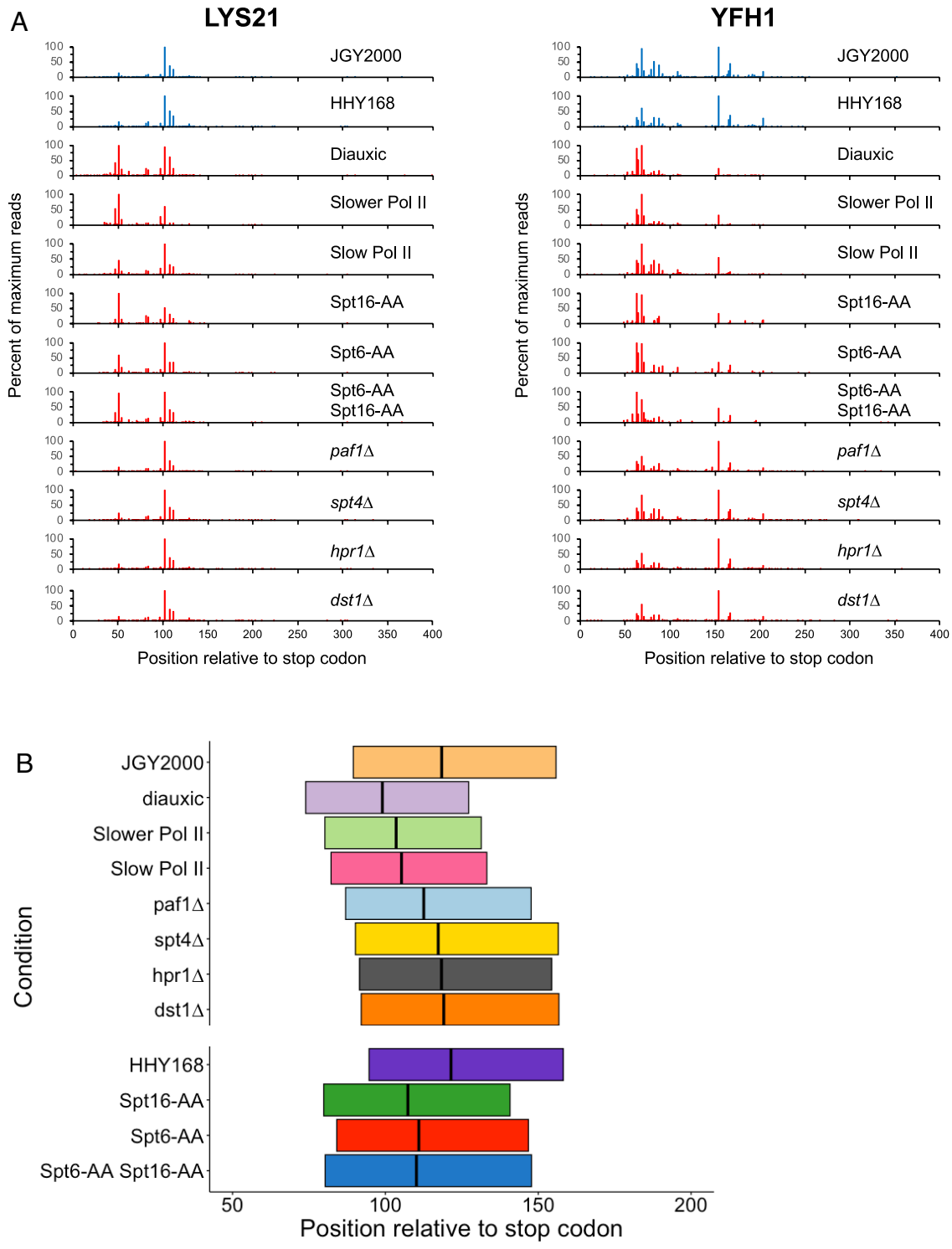

Fig. 1. Depletion of Spt6 or Spt16 causes an upstream-shifted poly(A) profile. (*A*) Poly(A) profiles of the *LYS21* and *YFH1* genes in the indicated genetic conditions. Individual isoforms are defined by the number of nucleotides downstream of the stop codon, and their vertical heights indicate the expression level, relative to a value of 100 being defined by the isoform with the highest number of reads under that condition. (*B*) Transcriptome-level location of poly(A) sites in the indicated strains. The left (5') and right (3') boundaries of each box represent median genome-wide values for the locations of the 10th and 90th percentile isoforms, and the vertical line represents the genome-wide 50th percentile position.

We also compared overall net shifts (a metric that represents the combined shift in polyadenylation at multiple positions between wild-type and genetically altered cells) of individual genes for all three conditions showing upstream-shifted poly(A) profiles. Interestingly, net shift correlations of slow Pol II mutants with either FACT-depleted or Spt6-depleted cells are modest (R ~ 0.3 to 0.4), whereas the correlation between FACT-depleted and Spt6-depleted cells (R = 0.67) is significantly higher and comparable to that of the correlation (0.66) between two slow Pol II mutants (Fig. 3*C*, lower left quadrants). Similarly, on an individual isoform basis, correlation of slow Pol II mutants vs. either FACT-depleted or Spt6-depleted cells (R ~ 0.6) is significantly lower than the correlation between FACT- depleted and Spt6-depleted (0.8) cells (*SI Appendix*, Fig. S1). There are many examples (a few shown in Fig. 3*D*) in which the magnitude of the upstream shifts is very different among the genetic conditions.

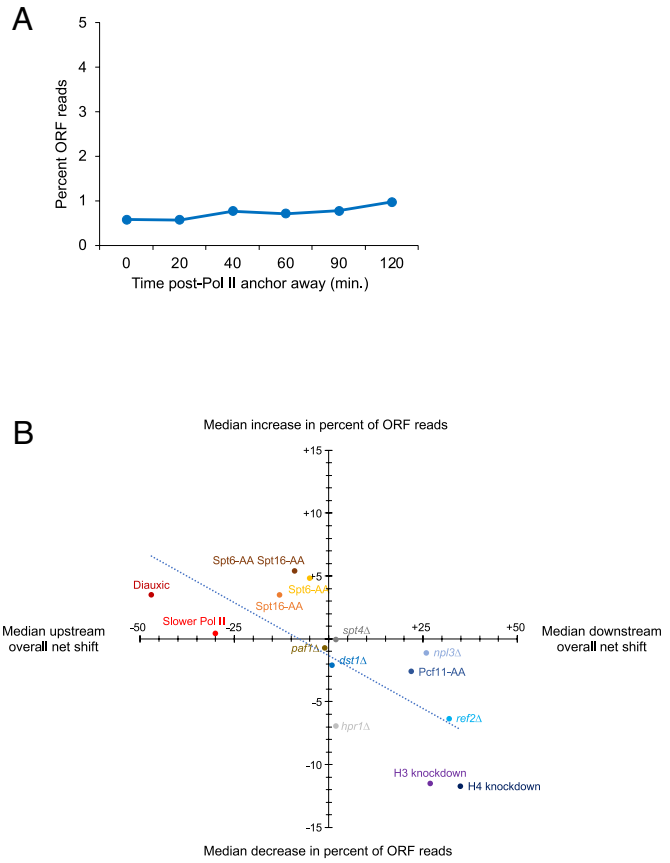

Fig. 2. Level of polyadenylation within coding regions is linked to poly(A) profiles in the 3′ UTR. (*A*) Percent of total reads for isoforms with poly(A) sites in the coding region for the indicated times after depleting Pol II via anchor-away. (*B*) Relationship between the net shift (downstream or upstream indicated on the *x*-axis) and the median increase or decrease in the percent of sequence reads for isoforms with poly(A) sites in the coding region (*y*-axis) for the indicated genetic conditions. The dotted trend line highlights the relationship between overall net shift and percent change in the coding region reads (R = −0.72, *P* = 0.0002).

These observations indicate that catalytically slow Pol II reduces the rate of Pol II elongation by a mechanism distinct from that of Spt6 and FACT depletion. The more similar effects of FACT and Spt6 depletion are suggestive of related effects of these histone chaperones on chromatin during Pol II elongation.

Atypical Genes with Downstream-Shifted Poly(A) Profiles Reveal Similarities between FACT and Spt6 but Strong Differences with Slow Pol II Derivatives. In previous work, we observed that 7% of genes showed atypical downstream-shifted poly(A) profiles in cells with slow Pol II derivatives (20). The genes with downstream-shifted poly(A) profiles are very similar, though not identical, in two different slow Pol II strains (20). Downstream-shifted poly(A) profiles occur in 11% of genes in FACT-depleted cells and 17% of Spt6-depleted cells (Fig. 3*A*).

Unlike the very strong overlap of genes with upstream-shifted poly(A) profiles in all three genetic conditions (Fig. 3*B*), there is no significant overlap in genes with downstream-shifted poly(A) profiles between slow Pol II cells and either FACT-depleted or Spt6-depleted cells (Fig. 4*A*). In contrast, genes with downstream-shifted or unshifted poly(A) profiles overlap considerably in Spt6-depleted and FACT-depleted cells (Fig. 4*B*). Examples in which a given gene shows an upstream-shifted poly(A) profile in one condition and a downstream shifted profile in another condition are shown in Fig. 4*C*. Thus, depletion of Spt6 or FACT cause related effects on Pol II elongation that differ from those caused by slow Pol II derivatives, indicating that a reduced Pol II elongation rate does not simply increase Pol II dwell time uniformly throughout the 3′ UTR.

FACT and Spt6 are similar, though not identical, in their effects on poly(A) profiles, presumably because both act through chromatin with some sequence specificity for histone deposition and/or eviction. In contrast, Pol II mutations that affect the elongation rate change the pattern of Pol II pausing and have different sequence preferences at Pol II pause sites (56). Thus, although reduced Pol II elongation rate generally causes upstream-shifted poly(A) profiles, sequence-specific effects on Pol II pausing and/or the local chromatin structure might underlie why FACT- and Spt6-depleted cells differ from slow Pol II cells.

Decreased Pol II Processivity Is Linked to Downstream-Shifted Poly(A) Profiles in FACT- and Spt6-Depleted Cells. We cannot directly measure the Pol II elongation rate in FACT- or Spt6-depleted cells because protein depletion by the anchor-away method is too slow. However, reduction of the Pol II elongation rate by genetic (Pol II mutants) or chemical (6-azauracil or mycophenolic acid) perturbations is associated with a defect in Pol II processivity (1). Reduced processivity is a hallmark of reduced elongation rate; the converse is not true. To provide independent evidence that depletion of FACT and Spt6 has reduced Pol II elongation rates, we examined Pol II processivity in genome-scale datasets of Pol II occupancy in FACT- and Spt6-depleted cells (same strains as used here) generated by Francois Robert and colleagues (17).

We measured Pol II occupancy near the 5′ and 3′ ends of coding regions greater than 1 kb in length. On an overall basis, when compared to wild-type cells, Pol II occupancy at 3′ ends is 11% (FACT depletion) or 7% (Spt6 depletion) lower than Pol II occupancy at 5′ ends (Fig. 5*A*, blue bars), directly demonstrating that depletion of FACT or Spt6 results in reduced processivity. This is typical of Pol II speed mutants. As a control, Pol II processivity defects are much smaller at adjacent regions in the center of coding regions (Fig. 5*A*, orange bars). These Pol II processivity defects almost certainly reflect decreased elongation rate upon FACT or Spt6 depletion, because a processivity defect per se is insufficient to cause an upstream-shifted poly(A) profile (1).

Unexpectedly, in both FACT- and Spt6-depleted cells, there is a link between decreased Pol II processivity and downstream-shifted poly(A) profiles. First, in a cohort of genes displaying a significant processivity defect (>2 SD from the median control region), downstream-shifted poly(A) profiles outnumber upstream-shifted profiles by a 2 to 1 margin (Fig. 5*B*). Second, based on median processivity (3′:5′ ratios of Pol II occupancy), genes with upstream-shifted poly(A) profiles have relatively higher levels of Pol II processivity (91%) than genes with downstream-shifted profiles (83%), and genes with unshifted profiles have intermediate levels (87%). Given the high likelihood that reduced Pol II processivity under conditions of FACT or Spt6 depletion reflects a reduced elongation rate, this result appears to conflict with the general result that decreased elongation rate is associated with upstream-shifted poly(A) profiles (*Discussion*).

Depletion of Histones Causes a Downstream-Shifted Poly(A) Profile. 3′ UTRs are largely sufficient to determine poly(A) profiles (57, 58), and unlike coding regions, they have long AT-rich stretches of DNA that may be important for restricting polyadenylation to 3′ UTRs (58). In principle, 3′ UTR recognition could occur at the DNA (AT-rich), RNA (AU-rich), or RNA:DNA hybrid (rU:dA- and/or rA:dT-rich) level (59). In one DNA-based model (59), elongating Pol II recognizes 3′ UTRs by their reduced nucleosome occupancy due to AT-rich sequences (60), which

A

	Diauxic	Slower Pol II	Spt16-AA	Spt6-AA	Spt6-AA Spt16-AA	*paf1Δ*	*dst1Δ*	*npl3Δ*	*ref2Δ*	Pcf11-AA	H3 knock-down	H4 knock-down
Shifted upstream	3,092 (91%)	2,596 (84%)	2,058 (75%)	1,763 (64%)	1,862 (69%)	1,814 (50%)	1,068 (31%)	428 (12%)	209 (6%)	262 (11%)	286 (8%)	106 (3%)
Shifted downstream	131 (4%)	205 (7%)	292 (11%)	460 (17%)	415 (15%)	1,007 (28%)	1,668 (49%)	2,650 (75%)	2,974 (83%)	1,804 (76%)	2,757 (82%)	3,231 (91%)
Unshifted	154 (5%)	225 (7%)	382 (14%)	500 (18%)	395 (15%)	740 (21%)	598 (18%)	382 (11%)	376 (11%)	281 (12%)	281 (8%)	223 (6%)
Other	27 (1%)	52 (2%)	24 (1%)	40 (1%)	40 (1%)	40 (1%)	75 (2%)	50 (1%)	18 (1%)	26 (1%)	41 (1%)	10 (< 1%)
Total	**3,404**	**3,078**	**2,756**	**2,763**	**2,712**	**3,601**	**3,409**	**3,510**	**3,577**	**2,373**	**3,365**	**3,570**

B

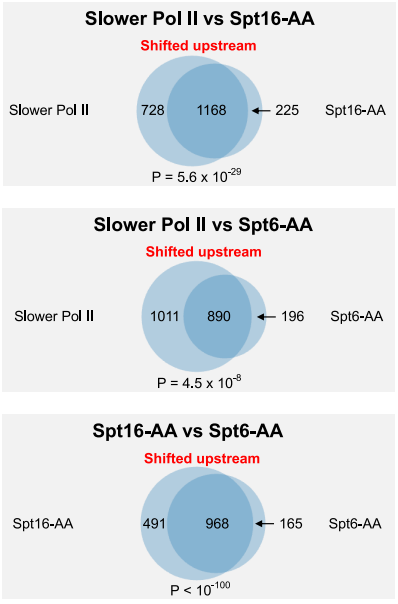

C

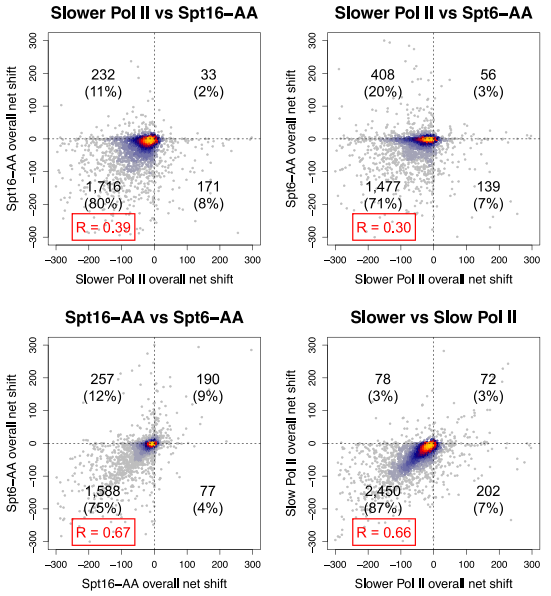

D

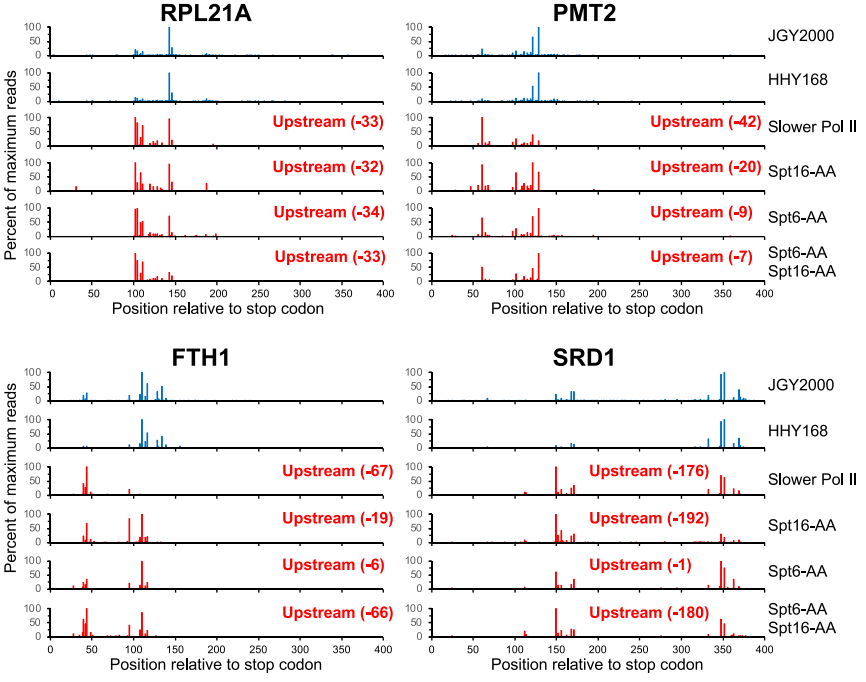

Fig. 3. Poly(A) profiles of strains with mutations in Pol II elongation factors. (*A*) Table listing the number of genes with upstream-shifted, downstream-shifted, or unshifted poly(A) profiles in the indicated strains. (*B*) Venn diagrams showing the overlap between genes with upstream-shifted poly(A) profiles in pairwise comparisons of slow Pol II, Spt6-depleted, and Spt16-depleted strains. The *P*-values represent the likelihood that the overlaps occur by chance. (*C*) Pairwise-comparison net poly(A) shifts of individual genes in slow Pol II, Spt6-depleted, and Spt16-depleted strains. (*D*) Examples of genes showing variations in the magnitudes of upstream-shifted poly(A) profiles in the indicated strains.

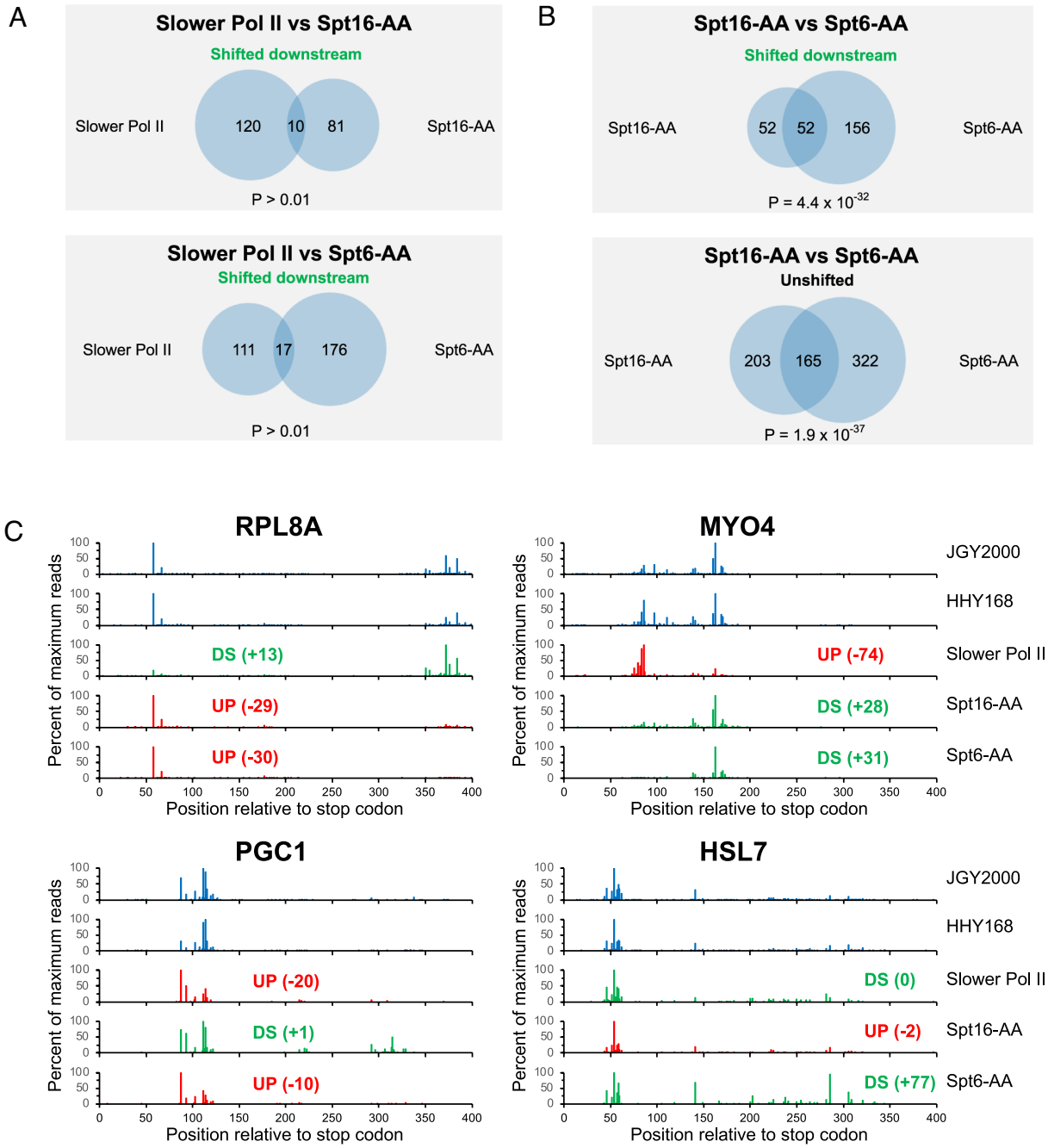

Fig. 4. Genes with downstream-shifted or unshifted poly(A) profiles vary across strains. (*A*) Venn diagrams showing the overlap between genes with downstream-shifted poly(A) profiles in pairwise comparisons of slow Pol II, Spt6-depleted, and Spt16-depleted strains. The *P*-values represent the likelihood that the overlaps occur by chance. (*B*) Venn diagrams showing the overlap between genes with downstream-shifted or unshifted poly(A) profiles in Spt16- and Spt6-depleted strains. (*C*) Examples of genes showing discordance between upstream- and downstream-shifted poly(A) profiles in the indicated strains.

results in dissociation of some elongation factors and subsequent recruitment of the cleavage/polyadenylation machinery. Such a model predicts that general histone depletion should lead to increased polyadenylation within coding regions and an upstream-shifted poly(A) profile.

In contradistinction to this model, depletion of either histone H3 or H4 via glucose-shutoff alleles (61) results in a dramatically downstream-shifted poly(A) profile (Fig. 6*A*) as well as a substantial decrease in the already-low level of polyadenylation within coding regions (Fig. 2*B*). Very few genes (3 to 8%; Fig. 3*A*) show an upstream-shifted profile in these histone-depleted strains. The poly(A) profile upon H3 or H4 depletion is considerably more downstream-shifted than observed in two fast Pol II strains (20), and this downstream shift in polyadenylation is roughly comparable in magnitude to the dramatic downstream shifts in strains lacking or depleted for Ref2, Npl3, or Pcf11, factors that are critical for functioning of the cleavage/polyadenylation machinery (Fig. 6*B*). Downstream-shifted poly(A) profiles in strains with defects in the cleavage/polyadenylation machinery have been observed previously (33, 62, 63). They are expected because inefficient cleavage at a given site is linked to inefficient termination, thereby allowing Pol II to travel further downstream and preferentially generate poly(A) sites at more distal locations.

Pairwise comparisons involving histone-depleted and cleavage/polyadenylation-defective strains reveal a significant overlap of genes showing downstream-shifted poly(A) profiles in all cases (Fig. 6*C* and *SI Appendix*, Fig. S2). This overlap is especially strong for the H3- and H4-depleted strains, even though the magnitudes of the

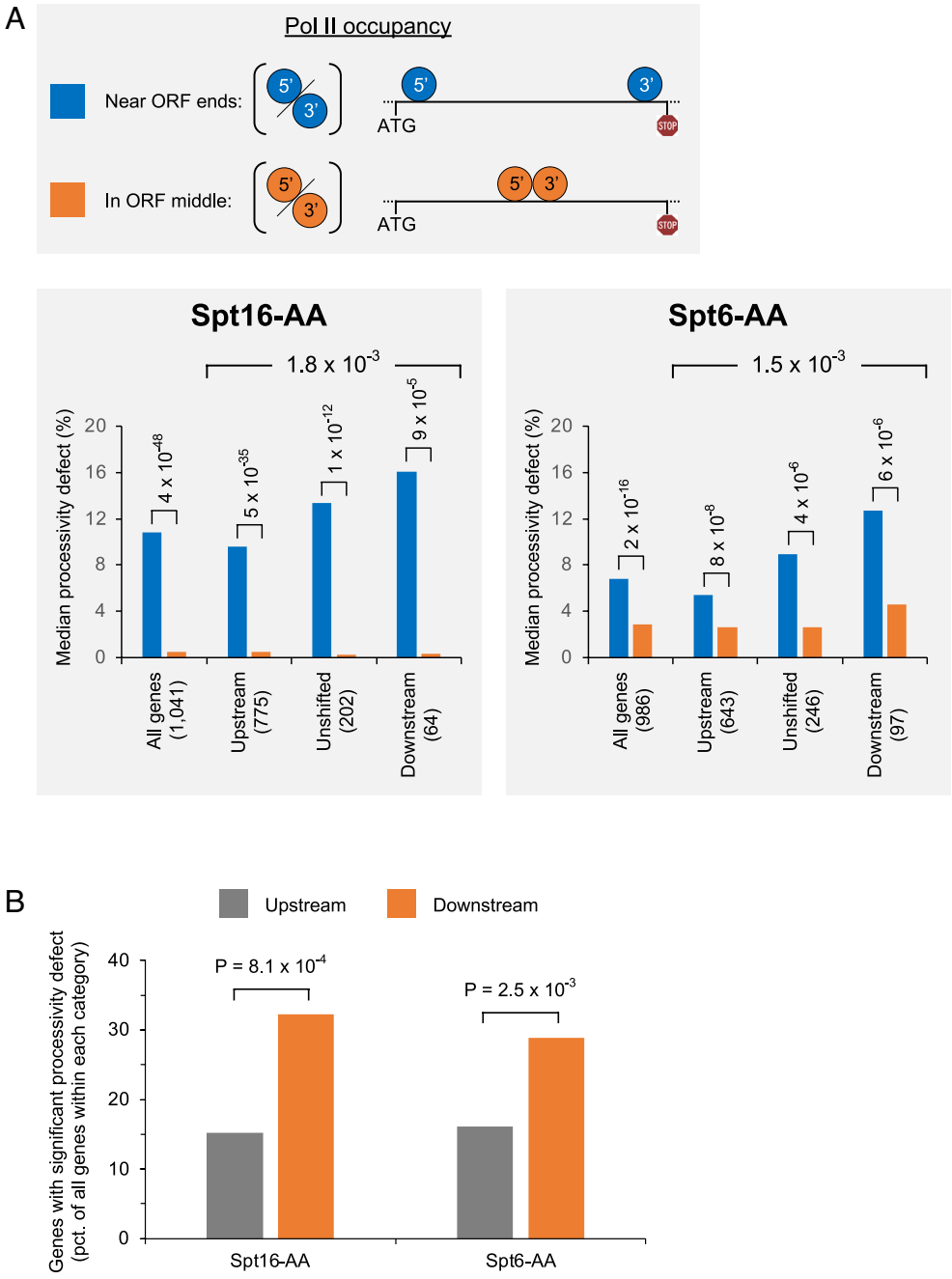

Fig. 5. Spt6 and Spt16 affect Pol II processivity. (*A*) Schematic showing that processivity is measured by relative levels of Pol II occupancy near 5′ and 3′ end (blue). As a control, relative levels of Pol II occupancy at adjacent locations in the middle of the genes (orange) are measured. Shown below are mean processivity defects (in percent) of genes with upstream-shifted, downstream-shifted, and unshifted poly(A) profiles in Spt6- and Spt16-depleted strains. The number of genes within each category is indicated in parentheses. (*B*) Percent of all genes with upstream-shifted or downstream-shifted poly(A) profiles that show a significant processivity defect.

downstream shifts are comparable to strains defective in the cleavage/polyadenylation machinery. This observation suggests that downstream shifts in polyadenylation caused by depletion of histone and cleavage/polyadenylation factors differ on a mechanistic level.

Discussion

Spt6 and FACT Are Required for Achieving the Physiological Rate of Pol II Elongation. Pol II derivatives with slow elongation rates confer an upstream-shifted poly(A) profile in yeast (20–22) and human (22–25) cells. Such upstream poly(A) shifts are due to Pol II elongation rate and not Pol II processivity (20). They reflect increased dwell time of elongating Pol II at individual nucleotides (22), thereby permitting preferential polyadenylation at upstream positions. As cleavage/polyadenylation initiates transcriptional termination and hence occurs only once per mRNA molecule, increased polyadenylation at upstream positions necessarily results in decreased polyadenylation at downstream positions.

Here we show that depletion of the histone chaperones FACT and Spt6 causes an upstream poly(A) shift at most genes. Both FACT (16) and Spt6 (64) travel with elongating Pol II and presumably affect chromatin structure throughout the entire gene. There is no evidence, and it is highly unlikely, that these histone chaperones affect the cleavage/polyadenylation machinery. Furthermore, the genes showing upstream-shifted poly(A) profiles in FACT- and

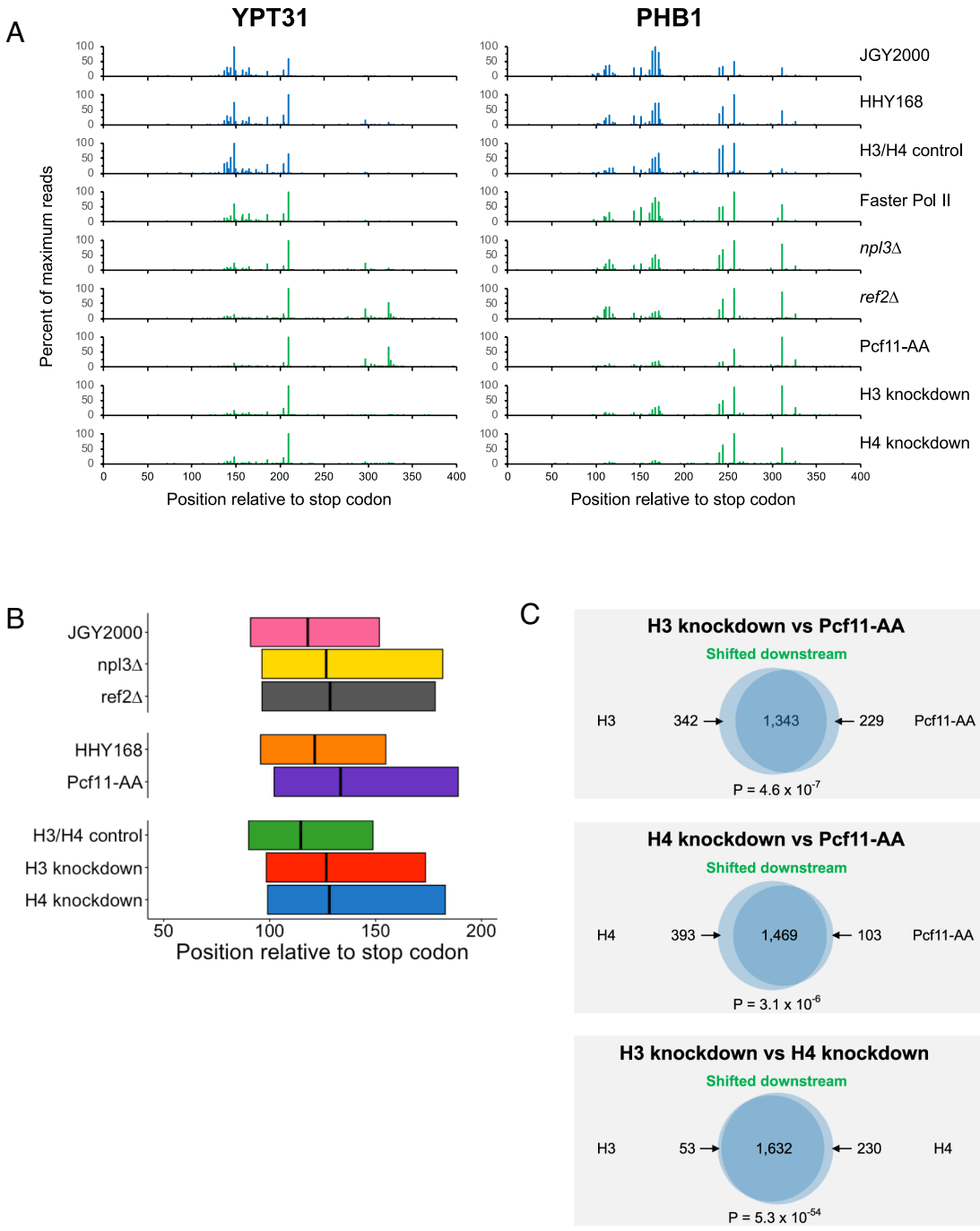

Fig. 6. Depletion of nucleosomes or cleavage/polyadenylation factors causes downstream-shifted poly(A) profiles. (*A*) Poly(A) profiles of the *YPT31* and *PHB1* genes in the indicated genetic conditions. Individual isoforms are defined by the number of nucleotides downstream of the stop codon, and their vertical heights indicate the expression level, relative to a value of 100 being defined by the isoform with the highest number of reads under that condition. (*B*) Transcriptome-level location of poly(A) sites in the indicated strains. The left (5′) and right (3′) boundaries of each box represent the locations of the median genome-wide values for the 10th and 90th percentile isoforms, and the vertical line represents the genome-wide 50th percentile position. (*C*) Venn diagrams showing the overlap between genes with downstream-shifted poly(A) profiles in pairwise comparisons of H3-, H4-, and Pcf11-depleted strains. The *P*-values represent the likelihood that the overlaps occur by chance.

Spt6-depleted cells are largely in common with those in slow Pol II cells, and most poly(A) profiles of upstream-shifted genes are highly correlated in the three conditions. These observations indicate that FACT and Spt6 are each required for achieving the physiological rate of Pol II elongation. This conclusion is strongly and independently supported by the overall Pol II processivity defect in FACT- and Spt6-depleted strains. Our results are consistent with the finding that Spt6 enhances the Pol II elongation rate in metazoans (19, 65), and they resolve the uncertainty about the role of FACT in stimulating the Pol II elongation rate (14, 19).

Molecular Implications of Gene Specificity. A minority of genes in FACT-depleted, Spt6-depleted, and slow Pol II cells show atypical downstream-shifted poly(A) profiles. Such gene-specific effects could be explained by several nonmutually exclusive mechanisms. First, 3′ UTR sequences might differ in Pol II pause sites and/or local elongation rate affecting Pol II dwell time. Second, sequence-specific differences in the local Pol II elongation rate could differentially affect the structure of the mRNA emerging from the elongation complex, resulting in preferential inhibition of upstream poly(A) site utilization. Third, as FACT and Spt6

facilitate nucleosome eviction and deposition, 3′ UTR-specific differences in nucleosome occupancy or stability could cause atypical downstream-shifted poly(A) profiles (see below).

Unexpectedly, in Spt6- and FACT-depleted cells, the minority of loci with reduced Pol II processivity are associated with more downstream-shifted poly(A) profiles. Reduced Pol II processivity in these depletion strains likely reflects slower Pol II speed, as opposed to some heretofore unknown aspect of processivity that does not affect poly(A) profiles. This suggests that at least some gene-specificity of poly(A) profiles reflects gene-specific differences in the Pol II elongation rate. Although the link between reduced Pol II processivity and downstream-shifted poly(A) profiles is subtle, it is significant.

To affect poly(A) profiles, gene-specific differences in the Pol II elongation rate must occur within the 3′ UTR. However, gene-specific differences in Pol II processivity (and hence elongation rate) occur throughout the coding region. It seems unlikely that DNA sequence differences in coding regions and 3′ UTRs of individual genes would be coordinated with respect to the Pol II elongation rate. Furthermore, in Spt6- and FACT-depleted cells, decreased Pol II elongation rate within coding regions is associated with downstream-shifted poly(A) profiles, which presumably reflect increased Pol II elongation rate in 3′ UTRs as well.

The apparent contradiction that slower Pol II elongation rate in the coding region is associated with faster elongation rate in the 3′ UTR suggests that the Pol II elongation machinery exists in two forms that differ in Pol II speed and hence processivity. If the slow form preferentially dissociates from the template as it travels through the coding region, atypical genes with lower levels of Pol II processivity/speed will have relatively higher levels of the fast form when Pol II reaches the 3′ UTR and hence cause a downstream shift in poly(A) sites. Though clearly speculative, this suggestion is consistent with increasing elongation rates as Pol II traverses the gene in mammalian cells (66) as well as substantial variability in elongation rate of individual Pol II molecules and a connection between Pol II density and mRNA cleavage efficiency in *Drosophila* cells (67).

It seems unlikely that gene-specificity of poly(A) profiles occurs solely at the 3′ UTR, as this would not easily explain why processivity/speed variation in coding regions influences poly(A) patterns. Gene-to-gene variation of Pol II speed might be due to sequences affecting Pol II pausing sites throughout coding regions (56) or to sequence differences early in the coding region (perhaps around the +1 nucleosome) that set the elongation rate that is propagated downstream. Alternatively, the Pol II elongation rate could be influenced at the promoter via compositional differences (subunit stoichiometry and/or modifications) in Pol II or associated proteins. In this regard, kinases recruited to promoters by activator proteins selectively travel through the coding regions of target genes (68, 69). These considerations do not exclude the role of 3′ UTR sequences in gene-specific poly(A) profiles.

Nucleosomes Inhibit the Pol II Elongation Rate In Vivo. While nucleosomes inhibit the Pol II elongation rate in vitro, the Pol II elongation rate in vivo is roughly comparable to the elongation rate of purified Pol II on naked DNA templates (70–73). This suggests that histone chaperones and perhaps other elongation factors overcome the otherwise strong inhibitory effects of nucleosomes. Thus, it is unclear how elongating Pol II would behave on nucleosome-depleted regions in vivo, and whether such regions would affect the poly(A) profile.

Our observations strongly suggest that nucleosomes inhibit the Pol II elongation rate in vivo, even in the presence of all Pol II elongation factors. Specifically, depletion of histone H3 or H4 causes greatly reduced polyadenylation within coding regions and a strong downstream-shifted poly(A) profile within 3′ UTRs. This observation is inconsistent with a DNA-based (AT-rich) model for preferential polyadenylation in the 3′ UTR vs. the coding region (59). Although the downstream shift upon histone depletion resembles that occurring in cells defective in cleavage/polyadenylation, it is highly unlikely that histones directly inhibit the activity of the cleavage/polyadenylation machinery. The opposite directions of poly(A) shifts caused by histone depletion vs. depletion of FACT or Spt6 that are important for histone eviction (12–14) demonstrates the importance of chromatin in affecting Pol II elongation rates and concomitant effects on poly(A) profiles.

Although the histone depletion described here represents an artificial condition, histone depletion appears to occur in aging yeast cells (74). In addition, local effects on nucleosome occupancy likely affect Pol II elongation in wild-type cells. Pol II occupancy at AT-rich regions just upstream of poly(A) sites is relatively reduced (22), perhaps reflecting local increased Pol II speed (75) due to lower histone occupancy at AT-rich regions (76). Nucleosomes have DNA sequence preferences (77–79) that might contribute to local changes in the Pol II elongation rate. These considerations suggest that gene-specific and local effects of FACT and Spt6 on nucleosome occupancy will affect poly(A) profiles.

Altered Chromatin Structure as a Potential Mechanism for Regulated Alternative Polyadenylation in Response to Genetic or Environmental Changes. Poly(A) site utilization can be regulated on a transcriptome scale by environmental or developmental conditions (26). Transcriptome-scale regulation of poly(A) profiles can be due to regulated expression or activity of components of cleavage/polyadenylation machinery (26, 33, 34). Our results provide strong evidence that altered chromatin structure, through its effects on the Pol II elongation rate, is another mechanism for regulating alternative polyadenylation. Many disease-causing mutations map to genes encoding chromatin-modifying components, and such mutations could alter the Pol II elongation rate and hence poly(A) profiles. Environmental conditions that affect one or more chromatin-related components could lead to the same effects (80). Finally, by analogy with inhibitors (1) and the yeast diauxic response (20), conditions that reduce nucleotide precursors or otherwise affect the Pol II elongation rate should lead to widespread effects on poly(A) profiles and hence biological phenotypes. This chromatin-based mechanism is not mutually exclusive with the cleavage/polyadenylation-based mechanism, and both could operate under a given physiological condition. Based on gene-specificity observed in all cases we examined, we predict that environmental or genetic conditions will have widespread effects yet differentially affect poly(A) profiles of individual genes.

Materials And Methods

Yeast Strains. A number of the yeast strains used in this paper have been described previously (17, 20, 61). The *PCF11* anchor-away strain YJ012 was provided by Yi Jin, and the histone H3 and H4 depletion strains (DCB 200.1 and DCB 220.1) (61) were provided by Kerry Bloom. *SPT6* and *SPT16* anchor away strains YFR1480 and YFR1478 (17) were provided by Francois Robert. JYZ39, the double anchor away (Spt16-AA/Spt6-AA) strain, was constructed by induction of mating-type switching of YFR1478 with galactose-inducible HO endonuclease (81), crossing the resulting *MAT***a** strain with YFR1480, and selection of a *MAT***a** haploid with both *SPT6-FRB-KanMX* and *SPT16-FRB-KanMX* after sporulation and tetrad dissection. Complete deletions of *PAF1*, *DST1*, *NPL3*, and *REF2* open reading frames were constructed by CRISPR (see *SI Appendix*, Table S1 for guide and repair sequences) using derivatives of pML104 (82) to supply Cas9 and guide RNA.

Cell Growth and RNA Preparation. Most strains were grown in 50 mL of YPD (yeast extract-peptone-dextrose) to OD_{600} = 0.3 to 0.4 at 30 °C. Anchor-away strains were grown in YPD to OD_{600}= 0.3 to 0.4 at 30 °C and then treated with

1 μM rapamycin for 1 h. Histone shutoff strains were grown in YP medium containing 2% galactose to OD_{600} = 0.3 to 0.4 at 30 °C and then an additional 3 h in YPD after removal of galactose-containing media by filtration. For each strain, total RNA was isolated from 15 to 25 mL of cells and purified using the hot acid phenol method followed by QIAGEN RNeasy as described (83). 3′ READS was performed with 25 μg of purified total RNA with 17 cycles of amplification (40). Barcoded libraries were quantified on an Agilent Bioanalyzer 2100, pooled, and sequenced on the Illumina NextSeq 500 platform. Datasets for JGY2000 grown in diauxic conditions, JZY5, JZY6, JZY27, JZY33, and JZY15 were published previously (20).

General Dataset Processing. Illumina datasets were treated as previously (20). In summary, fastq files were prepared for mapping by discarding reads with ambiguous bases, removing adapter sequences from read ends, and first counting and then removing consecutive initial T residues (representing terminal A residues of the RNA) from the read. Reads lacking initial T residues were discarded. The first 17 nt of each read after the initial Ts were mapped to the Sac cer 3 version of the *Saccharomyces cerevisiae* genome using Bowtie (84), allowing no mismatches and keeping only uniquely mapped results. Mapped reads were discarded unless they showed evidence of nontemplated terminal A bases: The number of consecutive initial Ts in the original read needed to be higher than the number of A residues encoded by the genome immediately adjacent to the mapped position. The remaining reads, representing bona fide poly(A) isoforms endpoint, were scaled to 25 M total per replicate or 50 M for combined A+B replicates. When looking at individual genes, isoforms in the 400 nt downstream of the stop codon are represented by abundance relative to the most frequently observed isoform in this window, which is set to 100.

Poly(A) Profiles and Important Terms. The analysis of polyadenylation sites in 3′ UTRs has been described previously (20). Briefly, reads were assigned to a gene's 3′ UTR if they mapped to a 400 nt window immediately downstream of its ORF. For each condition or strain, we combined reads from both biological replicates at each position in the 3′ UTR. Genes with <1,000 total reads in the 3′ UTR were excluded from further analysis. The 3′ isoform endpoint frequencies were tabulated for each 3′ UTR, setting the value of the most expressed isoform to 100 and linearly scaling reads in the other positions relative to this value. Thus, the overall isoform expression as a function of distance within the 3′ UTR constitutes a gene's poly(A) profile. Percentile coordinates (10th, 25th, 50th, 75th, and 90th) for each 3′ UTR represent the position at which the indicated percentage of reads lies at or upstream (i.e., if the 25th percentile coordinate is +80, 25 percent of all 3′ UTR reads occur at or before +80). When necessary, the assigned position represents an interpolated value between the two isoform endpoints below and above the percentile rank. The cumulative net shift represents the combined net shift at the 10th, 25th, 50th, 75th, and 90th percentile coordinates (20). For each gene, the net number of percentile coordinates shifted is the number of percentile coordinates shifted upstream vs. the control strain/condition minus the number of percentile coordinates shifted downstream vs. the control strain/condition (20).

Analysis of ORF Reads. ORF reads for a given gene were processed similarly to 3′ UTR reads but were mapped to genomic regions that span the coding sequences (for ~200 genes, this also includes introns). As there are relatively few reads at individual positions within the ORF, ORF reads at all positions were combined and then consolidated in biological replicates. For each gene, the overall percentage of ORF reads was computed by dividing the consolidated ORF reads by the total number of reads in ORF + 3′ UTR regions. To measure ORF polyadenylation during a Pol II shutoff, we first selected the 4,449 genes with ≥1,000 3′ UTR reads at the 0′ and 20′ time points from a previously published dataset (51). We computed the overall sums of all ORF or 3′ UTR reads each time point (0′, 20′, 40′, 60′, 90′ 120′) and determined the percent of reads mapping in the ORF as a function of time.

Classification of Genes by Poly(A) Profile Shift. Genes were categorized by their poly(A) profile shift relative to isogenic controls as either upstream shifted, downstream shifted or unshifted essentially as described (20). Briefly, each gene's poly(A) profile was compared relative to either an isogenic or a predepletion control as follows. Genes were classified as upstream shifted if they possessed both a negative overall net shift and if the net number of percentile coordinate positions (10th, 25th, 50th, 75th, and 90th) shifted upstream was ≥1. Genes were deemed downshifted if they contained both a positive overall net shift and if the net number of percentile coordinates shifted downstream was ≥ 1. Genes were called as unshifted if either the overall net shift or the net number of percentile coordinates shifted equaled zero.

Correlations of Biological Replicates and Isoform Expression Levels across Strains/Conditions. Reproducibility of biological replicates was assessed by pairwise comparisons of reads either in individual isoforms (20). All isoforms with ≥10 reads in both replicates (>50,000 isoforms per strain or condition) were selected and a Pearson correlation was computed for each set of replicates (*SI Appendix*, Fig. S1). To assay expression differences at the isoform level in various strains and conditions, we first combined the reads for each isoform in the two biological replicates in each of the 15 strains or condition. We then selected 29,148 isoforms which possessed a combined minimum of 10 or more reads in every strain or condition, $\log_{10}$-transformed the read values, and computed pairwise Pearson correlations for all possible combinations (*SI Appendix*, Fig. S1).

Genome-Wide Measurement of Spt16 and Spt6 Processivity. We computed processivity values using a published yeast Pol II occupancy tiled microarray dataset (GEO: GSE113270) (17) as follows. After mapping the probe coordinates onto the genome, we eliminated all genes with coding sequences <1,000 nt in length. For each gene within each dataset, we counted the number of probes whose midpoint coordinates are contained within either +100 to +300 relative to the ATG ("5′ region") or −300 to −100 relative to the stop codon ("3′ region"). If a gene contains ≥2 probes in each region in both biological replicates, we computed a 5′ region/3′ region processivity ratio by separately averaging the median Pol II occupancy values in the 5′ and 3′ regions in both replicates and then dividing the averaged 5′ region occupancy values by the averaged 3′ region occupancy values.

Processivity control regions for each gene were defined as −200 to −1 ("control 5′ region") and +1 to +200 ("control 3′ region") relative to the midpoint of the genomic fragment encompassing each coding sequence. Processivity ratios (control 5′ region/control 3′ region) were calculated exactly as described above. Actual and control 5′/3′ processivity ratios were converted to percent processivity defects by subtracting the reciprocal of each processivity ratio from 1 and multiplying the resulting value by 100.

Data, Materials, and Software Availability. Datasets for poly(A) profiles in the various mutant strains have been deposited in the NCBI GEO expression omnibus under accession number GSE262747. The analysis also uses poly(A) profile datasets previously deposited in GSE151196 (20) and GSE113270 (17). Datasets from Rpb1 depletion time courses (51) used for the half-life analysis were previously deposited in GSE52286.

ACKNOWLEDGMENTS. We thank Catherine Maddox for excellent technical assistance, Francois Robert for anchor-away strains for depleting Spt6 and Spt16, Kerry Bloom for histone-depletion strains, and Francois Robert, Fred Winston, and Steve Buratowski for useful discussion. This work was supported by a grant to K.S. from the NIH (GM 131801).

1. P. B. Mason, K. Struhl, Distinction and relationship between elongation rate and processivity of RNA polymerase II *in vivo*. *Mol. Cell* **17**, 831–840 (2005).
2. Y. Aoi, A. Shilatifard, Transcriptional elongation control in developmental gene expression, aging, and disease. *Mol. Cell* **83**, 3972–3999 (2023).
3. I. Jonkers, H. Kwak, J. T. Lis, Genome-wide dynamics of Pol II elongation and its interplay with promoter proximal pausing, chromatin, and exons. *Elife* **3**, e02407 (2014).
4. G. Dujardin *et al.*, How slow RNA polymerase II elongation favors alternative exon skipping. *Mol. Cell* **54**, 683–690 (2014).
5. I. Jonkers, J. T. Lis, Getting up to speed with transcription elongation by RNA polymerase II. *Nat. Rev. Mol. Cell. Biol.* **16**, 167–177 (2015).
6. L. Muniz *et al.*, Control of gene expression in senescence through transcriptional read-through of convergent protein-coding genes. *Cell Rep.* **21**, 2433–2446 (2017).
7. N. Fong *et al.*, Effects of transcription elongation rate and Xrn2 exonuclease activity on RNA polymerase II termination suggest widespread kinetic competition. *Mol. Cell* **60**, 256–267 (2015).
8. L. Muniz, E. Nicolas, D. Trouche, RNA polymerase II speed: A key player in controlling and adapting transcriptome composition. *EMBO J.* **40**, e105740 (2021).
9. A. Kristjuhan, J. Q. Svejstrup, Evidence for distinct mechanisms facilitating transcript elongation through chromatin in vivo. *EMBO J.* **23**, 4243–4252 (2004).
10. C. K. Lee, Y. Shibata, B. Rao, B. D. Strahl, J. D. Lieb, Evidence for nucleosome depletion at active regulatory regions genome-wide. *Nat. Genet.* **36**, 900–905 (2004).

11. M. A. Schwabish, K. Struhl, Evidence for eviction and rapid deposition of histones upon transcriptional elongation by RNA polymerase II. *Mol. Cell. Biol.* **24**, 10111–10117 (2004).
12. C. L. W. Miller, J. L. Warner, F. Winston, Insights into Spt6: A histone chaperone that functions in transcription, DNA replication, and genome stability. *Trends Genet.* **39**, 858–872 (2023).
13. F. Robert, C. Jeronimo, Transcription-coupled nucleosome assembly. *Trends Biochem. Sci.* **48**, 978–992 (2023).
14. C. Jeronimo, F. Robert, The histone chaperone FACT: A guardian of chromatin structure integrity. *Transcription* **13**, 16–38 (2022).
15. C. D. Kaplan, L. Laprade, F. Winston, Transcription elongation factors repress transcription initiation from cryptic sites. *Science* **301**, 1096–1099 (2003).
16. P. B. Mason, K. Struhl, The FACT complex travels with elongating RNA polymerase II and is important for the fidelity of transcriptional initiation *in vivo*. *Mol. Cell. Biol.* **23**, 8323–8333 (2003).
17. C. Jeronimo, C. Poitras, F. Robert, Histone recycling by FACT and Spt6 during transcription prevents the scrambling of histone modifications. *Cell Rep.* **28**, 1206–1218.e8 (2019).
18. H. Ehara, T. Kujirai, M. Shirouzu, H. Kurumizaka, S. I. Sekine, Structural basis of nucleosome disassembly and reassembly by RNAPII elongation complex with FACT. *Science* **377**, eabp9466 (2022).
19. M. B. Ardehali *et al.*, Spt6 enhances the elongation rate of RNA polymerase II in vivo. *EMBO J.* **28**, 1067–1077 (2009).
20. J. V. Geisberg, Z. Moqtaderi, K. Struhl, The transcriptional elongation rate regulates alternative polyadenylation in yeast. *eLife* **9**, e59810 (2020).
21. C. Yague-Sanz *et al.*, Nutrient-dependent control of RNA polymerase II elongation rate regulates specific gene expression programs by alternative polyadenylation. *Genes Dev.* **34**, 883–897 (2020).
22. J. V. Geisberg *et al.*, Nucleotide-level linkage of transcriptional elongation and polyadenylation. *eLife* **11**, e83153 (2022).
23. X. Liu *et al.*, Transcription elongation rate has a tissue-specific impact on alternative cleavage and polyadenylation in Drosophila melanogaster. *RNA* **23**, 1807–1816 (2017).
24. M. A. Cortazar *et al.*, Control of RNA Pol II speed by PNUTS-PP1 and Spt5 dephosphorylation facilitates termination by a "Sitting Duck Torpedo" mechanism. *Mol. Cell* **76**, 896–908.e4 (2019).
25. R. Goering *et al.*, LABRAT reveals association of alternative polyadenylation with transcript localization, RNA binding protein expression, transcription speed, and cancer survival. *BMC Genomics* **22**, 476 (2021).
26. S. Mitschka, C. Mayr, Context-specific regulation and function of mRNA alternative polyadenylation. *Nat. Rev. Mol. Cell. Biol.* **23**, 779–796 (2022).
27. R. Elkon, A. P. Ugalde, R. Agami, Alternative cleavage and polyadenylation: Extent, regulation and function. *Nat. Rev. Genet.* **14**, 496–506 (2013).
28. B. Tian, J. L. Manley, Alternative cleavage and polyadenylation: The long and short of it. *Trends Biochem. Sci.* **38**, 312–320 (2013).
29. L. Weill, E. Belloc, F. A. Bava, R. Mendez, Translational control by changes in poly(A) tail length: Recycling mRNAs. *Nat. Struct. Mol. Biol.* **19**, 577–585 (2012).
30. C. Mayr, D. P. Bartel, Widespread shortening of 3'UTRs by alternative cleavage and polyadenylation activates oncogenes in cancer cells. *Cell* **138**, 673–684 (2009).
31. J. Li, X. Lu, The emerging roles of 3′ untranslated regions in cancer. *Cancer Lett.* **337**, 22–25 (2013).
32. C. P. Masamha *et al.*, CFIm25 links alternative polyadenylation to glioblastoma tumour suppression. *Nature* **510**, 412–416 (2014).
33. A. Ogorodnikov *et al.*, Transcriptome 3'end organization by PCF11 links alternative polyadenylation to formation and neuronal differentiation of neuroblastoma. *Nat. Commun.* **9**, 5331 (2018).
34. K. Kamieniarz-Gdula *et al.*, Selective roles of vertebrate PCF11 in premature and full-length transcript termination. *Mol. Cell* **74**, 158–172 (2019).
35. J. Wittmeyer, L. Joss, T. Formosa, Spt16 and Pob3 of Saccharomyces cerevisiae form an essential, abundant heterodimer that is nuclear, chromatin-associated, and copurifies with DNA polymerase alpha. *Biochemistry* **38**, 8961–8971 (1999).
36. N. K. Brewster, G. C. Johnston, R. A. Singer, A bipartite yeast SSRP1 analog comprised of Pob3 and Nhp6 proteins modulates transcription. *Mol. Cell. Biol.* **21**, 3491–3502 (2001).
37. M. L. Diebold *et al.*, The structure of an Iws1/Spt6 complex reveals an interaction domain conserved in TFIIS, Elongin A and Med26. *EMBO J.* **29**, 3979–3991 (2010).
38. S. M. McDonald, D. Close, H. Xin, T. Formosa, C. P. Hill, Structure and biological importance of the Spn1-Spt6 interaction, and its regulatory role in nucleosome binding. *Mol. Cell* **40**, 725–735 (2010).
39. H. Haruki, J. Nishikawa, U. K. Laemmli, The anchor-away technique: Rapid, conditional establishment of yeast mutant phenotypes. *Mol. Cell* **31**, 925–932 (2008).
40. Y. Jin *et al.*, Mapping 3′ mRNA isoforms on a genomic scale. *Curr. Protoc. Mol. Biol.* **110**, 4.23.21–4.23.17 (2015).
41. C. Jeon, K. Agarwal, Fidelity of RNA polymerase II transcription controlled by elongation factor TFIIS. *Proc. Natl. Acad. Sci. U.S.A.* **93**, 13677–13682 (1996).
42. D. Kulish, K. Struhl, TFIIS enhances transcriptional elongation through an artificial arrest site *in vivo*. *Mol. Cell. Biol.* **21**, 4162–4168 (2001).
43. M. J. Thomas, A. A. Ptatas, D. K. Hawley, Transcriptional fidelity and proofreading by RNA polymerase II. *Cell* **93**, 627–637 (1998).
44. K. Strasser *et al.*, TREX is a conserved complex coupling transcription with mRNA export. *Nature* **417**, 304–307 (2002).
45. A. M. Francette, S. A. Tripplehorn, K. M. Arndt, The Paf1 complex: A keystone of nuclear regulation operating at the interface of transcription and chromatin. *J. Mol. Biol.* **433**, 166979 (2021).
46. N. J. Krogan *et al.*, The Paf1 complex is required for histone H3 methylation by COMPASS and Dot1. Linking transcriptional elongation to histone methylation. *Mol. Cell* **11**, 721–729 (2003).
47. H. H. Ng, S. Dole, K. Struhl, The Rtf1 component of the Paf1 transcriptional elongation complex is required for ubiquitination of histone H2B. *J. Biol. Chem.* **278**, 33625–33628 (2003).
48. Z. Moqtaderi, J. V. Geisberg, Y. Jin, X. Fan, K. Struhl, Species-specific factors mediate extensive heterogeneity of mRNA 3′ ends in yeasts. *Proc. Natl. Acad. Sci. U.S.A.* **110**, 11073–11078 (2013).
49. F. Ozsolak *et al.*, Comprehensive polyadenylation site maps in yeast and human reveal pervasive alternative polyadenylation. *Cell* **143**, 1018–1029 (2010).
50. V. Pelechano, W. Wei, L. M. Steinmetz, Extensive transcriptional heterogeneity revealed by isoform profiling. *Nature* **497**, 127–131 (2013).
51. J. V. Geisberg, Z. Moqtaderi, X. Fan, F. Ozsolak, K. Struhl, Global analysis of mRNA isoform half-lives reveals stabilizing and destabilizing elements in yeast. *Cell* **156**, 812–824 (2014).
52. S. Connelly, J. L. Manley, A functional mRNA polyadenylation signal is required for transcription termination by RNA polymerase II. *Genes Dev.* **2**, 440–452 (1988).
53. M. Kim *et al.*, The yeast Rat1 exonuclease promotes transcription termination by RNA polymerase II. *Nature* **432**, 517–522 (2004).
54. S. West, N. Gromak, N. J. Proudfoot, Human 5′ –> 3′ exonuclease Xrn2 promotes transcription termination at co-transcriptional cleavage sites. *Nature* **432**, 522–525 (2004).
55. W. Luo, A. W. Johnson, D. L. Bentley, The role of Rat1 in coupling mRNA 3′-end processing to transcription termination: Implications for a unified allosteric-torpedo model. *Genes Dev.* **20**, 954–965 (2006).
56. A. Khitun *et al.*, Elongation rate of RNA polymerase II affects pausing patterns across 3′ UTRs. *J. Biol. Chem.* **299**, 105289 (2023).
57. O. Shalem *et al.*, Systematic dissection of the sequence determinants of gene 3′ end mediated expression control. *PLoS Gene.* **11**, e1005147 (2015).
58. K. H. Lui, J. V. Geisberg, Z. Moqtaderi, K. Struhl, 3′ untranslated regions are modular entities that determine polyadenylation profiles. *Mol. Cell. Biol.* **42**, e0024422 (2022).
59. K. Struhl, How is polyadenylation restricted to 3′ untranslated regions? *Yeast* **41**, 186–191 (2024).
60. X. Fan *et al.*, Nucleosome depletion in yeast terminator regions is not intrinsic and can occur by a transcriptional mechanism linked to 3′ end formation. *Proc. Natl. Acad. Sci. U.S.A.* **107**, 17945–17950 (2010).
61. D. C. Bouck, K. Bloom, Pericentric chromatin is an elastic component of the mitotic spindle. *Curr. Biol.* **17**, 741–748 (2007).
62. W. Li *et al.*, Systematic profiling of poly(A)+ transcripts modulated by core 3′ end processing and splicing factors reveals regulatory rules of alternative cleavage and polyadenylation. *PLoS Genet.* **11**, e1005166 (2015).
63. B. Lackford *et al.*, Fip1 regulates mRNA alternative polyadenylation to promote stem cell self-renewal. *EMBO J.* **33**, 878–889 (2014).
64. E. D. Andrulis, E. Guzman, P. Doring, J. Werner, J. T. Lis, High-resolution localization of *Drosophila* Spt5 and Spt6 at heat shock genes in vivo: Roles in promoter proximal pausing and transcription elongation. *Genes Dev.* **14**, 2635–2649 (2000).
65. A. Narain *et al.*, Targeted protein degradation reveals a direct role of SPT6 in RNAPII elongation and termination. *Mol. Cell* **81**, 3110–3127 (2021).
66. C. G. Danko *et al.*, Signaling pathways differentially affect RNA polymerase II initiation, pausing, and elongation rate in cells. *Mol. Cell* **50**, 212–222 (2013).
67. J. Liu *et al.*, Real-time single-cell characterization of the eukaryotic transcription cycle reveals correlations between RNA initiation, elongation, and cleavage. *PLoS Comput. Biol.* **17**, e1008999 (2021).
68. M. Proft *et al.*, The stress-activated Hog1 kinase is a selective transcriptional elongation factor for genes responding to osmotic stress. *Mol. Cell* **23**, 241–250 (2006).
69. D. K. Pokholok, J. Zeitlinger, N. M. Hannett, D. B. Reynolds, R. A. Young, Activated signal transduction kinases frequently occupy target genes. *Science* **313**, 533–536 (2006).
70. D. Kennell, H. Riezman, Transcription and translation initiation frequencies of the *Escherichia coli lac* operon. *J. Mol. Biol.* **114**, 1–21 (1977).
71. C. T. Martin, J. E. Coleman, Kinetic analysis of T7 RNA polymerase-promoter interactions with small synthetic promoters. *Biochemistry* **26**, 2690–2696 (1987).
72. T. O'Brien, J. T. Lis, Rapid changes in *Drosophila* transcription after an instantaneous heat shock. *Mol. Cell. Biol.* **13**, 3456–3463 (1993).
73. V. Iyer, K. Struhl, Absolute mRNA levels and transcriptional initiation rates in *Saccharomyces cerevisiae*. *Proc. Natl. Acad. Sci. U.S.A.* **93**, 5208–5212 (1996).
74. J. Feser *et al.*, Elevated histone expression promotes life span extension. *Mol. Cell* **39**, 724–735 (2010).
75. A. H. Ehrensberger, G. P. Kelly, J. Q. Svejstrup, Mechanistic interpretation of promoter-proximal peaks and RNAPII density maps. *Cell* **154**, 713–715 (2013).
76. H. E. Peckham *et al.*, Nucleosome positioning signals in genomic DNA. *Genome Res.* **17**, 1170–1177 (2007).
77. H. R. Drew, A. A. Travers, DNA bending and its relation to nucleosome positioning. *J. Mol. Biol.* **186**, 773–790 (1985).
78. S. C. Satchwell, H. R. Drew, A. A. Travers, Sequence periodicities in chicken nucleosome core DNA. *J. Mol. Biol.* **191**, 659–675 (1986).
79. P. T. Lowary, J. Widom, New DNA sequence rules for high affinity binding to histone octamer and sequence-directed nucleosome positioning. *J. Mol. Biol.* **276**, 19–42 (1998).
80. K. Kaczmarek Michaels, S. Mohd Mostafa, J. Ruiz Capella, C. L. Moore, Regulation of alternative polyadenylation in the yeast Saccharomyces cerevisiae by histone H3K4 and H3K36 methyltransferases. *Nucl. Acids Res.* **48**, 5407–5425 (2020).
81. I. Herskowitz, R. E. Jensen, Putting the *HO* gene to work: Practical uses for mating-type switching. *Meth. Enzymol.* **194**, 132–146 (1991).
82. M. F. Laughery *et al.*, New vectors for simple and streamlined CRISPR-Cas9 genome editing in Saccharomyces cerevisiae. *Yeast* **32**, 711–720 (2015).
83. Z. Moqtaderi, J. V. Geisberg, K. Struhl, Extensive structural differences of closely related 3′ mRNA isoforms: Links to Pab1 binding and mRNA stability. *Mol. Cell* **72**, 849–861 (2018).
84. B. Langmead, C. Trapnell, M. Pop, S. L. Salzberg, Ultrafast and memory-efficient alignment of short DNA sequences to the human genome. *Genome Biol.* **10**, R25 (2009).